



## Full Length Article

Electronic structure and optical spectra of  $\text{Au}^-$  ions in RbCl

José Luis Pascual

Departamento de Química Física Aplicada, Universidad Autónoma de Madrid, 28049, Madrid, Spain

## ARTICLE INFO

## Keywords:

$\text{Au}^-$  ions  
RbCl  
Theoretical  
Absorption  
Emission

## ABSTRACT

*Ab initio* wavefunction based quantum chemical calculations on the electronic structure and optical spectra of  $\text{Au}^-$  ions in RbCl crystals are reported in this work.  $ns^2$  impurities in alkali halides are prototypical phosphor materials and have been extensively studied. In particular,  $\text{RbCl}:\text{Au}^-$  has been recently studied experimentally, but some points of the interpretation of the spectra are still controversial. Our calculations, that include all the major interactions present in the system, show very good agreement with the experimental findings. The calculations show that the levels belonging to the  $5d^9 6s^2 6p$  electron configuration lie relatively low in energy, and extensive mixing with some of the  $6s 6p$  levels is found. Large mixing of singlet and triplet states via spin-orbit coupling is found for most of the calculated levels. Due to this, band C in the absorption spectrum is found to consist of two transitions, to the  $2\text{ T}_{1u}$  and  $3\text{ T}_{1u}$  electronic levels, described as configurational mixtures of  $6s 6p\text{-}^1\text{P}_1$  and  $5d^9 6s^2 6p$  levels. Transitions to  $5d^9 6s^2 6p$  levels are found to be responsible for the D absorption bands of the material. On the other hand, emission band C' is assigned to a transition from the  $1\text{ A}_{2u}$  ( $5d^9 6s^2 6p$ ) electronic level to the ground level, a transition that is electric dipole forbidden. This level lies just below the levels responsible of the C absorption (around  $200\text{ cm}^{-1}$ ). These findings can justify the complex behavior of this C' emission.

## 1. Introduction

For a long time, alkali halide crystals doped with impurity ions which have the  $ns^2$  electronic configuration were considered the archetypal phosphors. This was due to a combination of the properties of the host alkali halides, namely, the high ionicity of the crystals, the large band gap that is present in their electronic structure, the relatively low melting temperatures and the relative simplicity of their cubic structures, and the impurity ions, that present the simple  $ns^2$  ground state configuration. After the pioneering experimental work of Hilsch [1] and the first detailed explanation of the properties of this family of phosphors, given by Seitz [2], an extensive number of experimental and theoretical studies have been carried out, making these phosphors among the best understood phosphors. However, this initial simplicity hid a large number of complexities and complications that were explained only later and some remain a challenge even now. Several reviews have been published that covered this topic [3–5]. These reviews focused mainly on the optical properties of cationic  $ns^2$  impurities (such as  $\text{Tl}^+$ ,  $\text{In}^+$ , and  $\text{Pb}^{2+}$ ).

On the other hand, the anionic  $ns^2$  centers (such as  $\text{Cu}^-$ ,  $\text{Ag}^-$ , and  $\text{Au}^-$ ) have been comparatively less studied. Among them,  $\text{Au}^-$  centers present several characteristic spectral features that make them more at-

tractive. Similar to other  $ns^2$  centers,  $\text{Au}^-$ -doped alkali halides exhibit several absorption bands called A, B, C, and D, in order of increasing energy. In fact, several D bands are found for  $\text{Au}^-$  ions [6–8]. The A, B, and C absorption bands are assigned to intraionic  $6s^2 \rightarrow 6s 6p$  transitions, similar to the rest of the  $ns^2$  centers; however, the D bands are supposed to have a different origin than in the cationic  $ns^2$  ions. This origin is still controversial: they have been assigned to intraionic  $5d^{10} 6s^2 \rightarrow 5d^9 6s^2 6p$  or  $6s^2 \rightarrow 6s 7p$  transitions [6–8]. A low intensity absorption band (usually called d absorption band) appears at the low energy tail of the C absorption band, whose origin is uncertain [8,9]. When excited into these excited states, radiative transitions back into the ground state take place, and several luminescence bands are recorded and they are referred to as A', B' and C' bands. The C' luminescence band characteristics (position, decay time constant) are somewhat unexpected and several explanations have been proposed, although a conclusive answer is still lacking [7,8]. The electron-phonon interaction is weaker than in other  $ns^2$ -doped alkali halides and this reflects in the appearance of zero phonon lines and vibronic structure in A and C bands [7]. A fourth luminescence band, referred to as  $\alpha$ , is found at lower energies than the A' band [7,8].  $\text{Au}^-$  centers in RbCl crystals have been the subject of recent experimental work in order to give some insights into these spe-

E-mail address: [josepascual@uam.es](mailto:josepascual@uam.es).<https://doi.org/10.1016/j.jlumin.2023.120207>

Received 1 August 2023; Received in revised form 8 September 2023; Accepted 19 September 2023

Available online 22 September 2023

0022-2313/© 2023 The Author(s). Published by Elsevier B.V. This is an open access article under the CC BY-NC-ND license (<http://creativecommons.org/licenses/by-nc-nd/4.0/>).

cial characteristics, but some of these facts are still not conclusively explained [8].

*Ab initio* molecular-orbital calculations have been thought to be able to provide detailed information about the ground and excited states of inorganic phosphors that can help in solving numerous problems related to them [10]. This kind of calculations were described as difficult and considered to require a long-taking effort [10]. In order to provide this helpful information, *ab initio* methods should be able to calculate states localized around the impurity center under the influence of the host crystal; to consider relativistic effects (both spin-independent and spin-dependent) which are central for heavy-element activators; to deal with the multiconfigurational nature of the excited manifolds of the dopant ions by treating the static correlation effects; and to include dynamic electron correlation effects as well (and its interplay with spin-orbit interaction). All these effects should be considered with an equivalent level of accuracy. Fortunately, nowadays tools suited to deal with these requisites are available and ready to be used. They consist in Douglas-Kroll-Hess relativistic multiconfigurational embedded cluster *ab initio* calculations [11]. Recent examples of their application can be found for lanthanides [11], transition metal ions [12] and other impurity ions [13].

With these ideas in mind, we present in this work the results of *ab initio* model potential (AIMP) embedded cluster wave function quantum mechanical calculations on the electronic structure of the  $\text{Au}^-$  center as a dopant in  $\text{RbCl}$  crystals. These calculations include all the major effects present in the system. Using these calculations, we can shed some light into the intricacies of the  $\text{Au}^-$  ions embedded in alkali halide hosts mentioned above. The details of the calculations are presented in Sec. 2, the results are presented and discussed in Sec. 3 and the conclusions of the work are presented in Sec. 4.

## 2. Details of the calculations

In this work, we present a theoretical study of the electronic properties of  $\text{Au}^-$  centers in  $\text{RbCl}$ , that can be described as wavefunction-based *ab initio* embedded cluster calculations. They have been performed using standard quantum chemistry molecular methods, based in multiconfigurational wavefunctions, able to describe electron correlation (both nondynamical and dynamical) [14–20] as well as scalar and spin-orbit coupling relativistic effects [21–24]. To represent the quantum mechanical interaction between the  $\text{Au}^-$  center and the embedding  $\text{RbCl}$  lattice, we have used the AIMP embedded cluster method [25,26]. Descriptions and applications of these methods can be found in the literature, here we describe the details necessary to reproduce the calculations. All the calculations presented in this work have been performed using MOL-CAS [27].

Pure  $\text{RbCl}$  crystalizes in the rocksalt structure, point group 225,  $\text{O}_h^5$  ( $Fm\bar{3}m$ ),  $a_0 = 6.5898 \text{ \AA}$  [28,29]. In  $\text{Au}^-$ -doped crystals,  $\text{Au}^-$  ions substitute for a  $\text{Cl}^-$  ion. The nearest neighbors are an octahedron of  $\text{Rb}^+$  ions and the next-nearest neighbors are 12  $\text{Cl}^-$  ions located at  $(\frac{1}{2}, \frac{1}{2}, 0)$ . Then, in order to study the material, we have chosen a  $(\text{AuRb}_6\text{Cl}_{12})^{7-}$  cluster properly embedded to represent the effects of the surrounding  $\text{RbCl}$  lattice. All calculations on the  $(\text{AuRb}_6\text{Cl}_{12})^{7-}$  cluster were all-electron calculations, with atomic natural orbital (ANO) basis sets for gold [30], rubidium [31], and chlorine [32], with respective contractions  $(24s21p15d11f4g2h)/[9s7p6d4f3g1h]$ ,  $(23s19p11d4f)/[6s5p3d1f]$ , and  $(17s12p5d)/[4s3p1d]$ . This basis set has been extended to include functions located at the  $(1,0,0)$   $\text{Cl}^-$  lattice sites. This type of functions is used to improve the orthogonality between the cluster MOs and the external crystal ion wavefunctions and, according to the recipes of Refs. [33] and [26], have been built using the outermost s and p occupied orbitals of the embedded  $\text{Cl}^-$  ion, totally contracted as  $(17s12p)/[1s1p]$ . The total number of basis set functions is 624.

The influence of the surrounding  $\text{RbCl}$  lattice in the  $(\text{AuRb}_6\text{Cl}_{12})^{7-}$  cluster has been taken into account by means of the *ab initio* model potential (AIMP) method [25,26]. The embedding potential of  $\text{RbCl}$

has been obtained in this work. The total-ion embedding AIMP representing the  $\text{Cl}^-$  anions and  $\text{Rb}^+$  cations have been produced via self-consistent embedded ion all-electron HF calculations [26] on  $\text{RbCl}$ . In these calculations, we have used ANO-RCC basis sets for Cl [32] and Rb [31], contracted as  $[8s7p5d4f]$  and  $[10s10p5d4f]$ , respectively. The total embedding potential is made of (1) total-ion model potentials for all ions located within a cube of  $7 \times 7 \times 7$  unit cells centered on  $\text{Cl}^-$ , a total of 3356 model potentials, and (2) a set of 12250 additional point charges situated at lattice sites, generated by the zero-multipole method of Gellé and Lepetit, [34] which closely reproduces the Ewald potential [35] within the cluster. The embedding potential is available from the author upon request.

The embedded cluster calculations are two-step spin-orbit coupling SA-CASSCF/MS-CASPT2/RASSI-SO DKH calculations. In the first step, we used the many-electron scalar relativistic second-order Douglas-Kroll-Hess (DKH) Hamiltonian [21,22]. Using it, we performed state-averaged complete-active-space self-consistent-field (SA-CASSCF) [14–16] calculations. The active space resulted from distributing 12 electrons in the 15 molecular orbitals of main Au 5d, 6s, 6p, 6d, and 7s character. The molecular orbitals have been optimized in separate SA-CASSCF calculations, except for the ground state  $6s^2 \text{ } ^1\text{A}_{1g}$ , that was individually optimized. (All calculations were done using  $D_{2h}$  symmetry) For the multiplets coming from the  $6s6p$  and  $5d^96s^26p$  electron configurations we have performed separate minimizations of the average energies of: one  $^1\text{A}_{2u}$  and one  $^1\text{E}_u$ ; three  $^1\text{T}_{1u}$  and two  $^1\text{T}_{2u}$ ; one  $^3\text{A}_{2u}$  and one  $^3\text{E}_u$ ; three  $^3\text{T}_{1u}$  and two  $^3\text{T}_{2u}$  multiplets. These SA-CASSCF calculations provided occupied and virtual molecular orbitals to feed subsequent multistate second-order perturbation theory calculations (MS-CASPT2) [17–20], in which dynamic electron correlation is taken into account. The Au 5d, 6s, Rb 4s, 4p, and Cl 3s, 3p electrons were explicitly included in the calculation, a total of 156 electrons. In order to avoid symmetry breakings in the MS-CASPT2 step, we have made calculations over the states of some  $\text{O}_h$  irrep separately. That is, we have calculated separately the  $^1\text{A}_{2u}$  and the 2  $^1\text{E}_u$  states (and similar with the triplets). The  $^1\text{T}_{1u}$  and  $^1\text{T}_{2u}$  (and the corresponding triplets) have been calculated together. The standard IPEA value [36] (0.25 au.) was used. In order to avoid the presence of intruder states, an extra imaginary shift [37] of 0.10 au. was used in the calculations.

In the second step, we included spin-orbit coupling effects by adding the atomic mean field integral (AMFI) approximation of the DKH spin-orbit coupling operator [23] to the scalar relativistic Hamiltonian. In this step, in order to combine spin-orbit couplings calculated with statically correlated wavefunctions and spin-orbit free energies that include dynamic correlation, we used the spin-free state shifting operator [38]. Accordingly, we performed restricted-active-space state-interaction spin-orbit calculations (RASSI-SO) [24] using the first-order corrected wavefunctions and the energies of the MS-CASPT2 procedure. All the states coming from the calculated spin free multiplets are allowed to couple in this step.

Using the computed wavefunctions and transition energies, the oscillator strengths and A Einstein coefficients of the allowed transitions are calculated [39,40]. In vacuo radiative lifetimes of the excited states ( $\tau_0$ ) are calculated as the inverse of the A coefficients. These values are corrected including standard local field corrections [41,42] calculated with a refraction index of  $\text{RbCl}$   $n = 1.4936$  [29] (corrected radiative lifetimes,  $\tau$ )

## 3. Results and discussion

The spin-orbit coupling in the 6s and 6p shells of the gold atom is so large that the electronic structure of the  $\text{RbCl}:\text{Au}^-$  material can only be understood at the spin-orbit coupling level. However, it is convenient to study first the electronic structure at the spin-orbit free level and, then, include the spin-orbit coupling effects. We report the results of MS-CASPT2 spin-orbit free calculations in Table 1. In the Table, we present the optimized local structure and spectroscopic parameters of

**Table 1**

Calculated spectroscopic constants of the  $6s^2$ ,  $6s6p$  and  $5d^96s^26p$  multiplets of the  $\text{Au}^-$  center in  $\text{RbCl}$ . Spin-orbit free MS-CASPT2 calculations. Au-Rb equilibrium distances,  $R_e$ , in Å; totally symmetric vibrational frequencies,  $\nu_{a1g}$ , in  $\text{cm}^{-1}$ ; minimum-to-minimum transition energies,  $T_e$ , in eV.

Multiplet	$R_e$	$\nu_{a1g}$	$T_e$
1 $^1A_{1g}$	3.420	81	0
1 $^3T_{1u}$	3.486	78	4.383
1 $^1T_{1u}$	3.470	76	5.265
1 $^3A_{2u}$	3.523	81	6.120
2 $^3T_{1u}$	3.539	83	6.151
1 $^3T_{2u}$	3.526	81	6.198
3 $^3T_{1u}$	3.511	80	6.217
1 $^1A_{2u}$	3.534	81	6.351
2 $^1T_{1u}$	3.531	80	6.389
1 $^1T_{2u}$	3.532	80	6.416
1 $^1E_u$	3.534	80	6.511
2 $^1T_{2u}$	3.533	80	6.537
1 $^3E_u$	3.535	81	6.615
2 $^3T_{2u}$	3.532	80	6.681
3 $^1T_{1u}$	3.525	80	6.986

the  $(\text{AuRb}_6\text{Cl}_{12})^{7-}$  cluster in the states belonging to the different multiplets related to the  $6s^2$ ,  $6s6p$  and  $5d^96s^26p$  electron configurations. We present equilibrium Au-Rb distances, breathing mode vibrational wavenumbers ( $a_{1g}$  symmetry) of the cluster and minimum-to-minimum electronic transition energies relative to the ground  $^1A_{1g}$  state.

Only the totally symmetrical breathing mode has been taken into account for the optimization of the cluster geometries. Our aim is to build a configuration coordinate energy diagram that can provide coarse information about the relative positions of the different energy levels. In this diagram, only one vibrational coordinate is used and usually, the  $a_{1g}$  breathing mode is the choice selected for these  $O_h$  octahedral clusters. With this strategy, finer details such as Jahn-Teller effects are missed, as they demand the use of several vibrational coordinates. Excited levels will, in general, present this kind of effects, but our hypothesis is that the fundamental information about the spectra can be obtained from the  $a_{1g}$  configuration coordinate diagram. Experiments on  $\text{KCl}:\text{Au}^-$  [43] conclude that the breathing mode is mostly responsible for the shape of the absorption A band. Moreover, the spin-orbit effects are considered to be much larger than Jahn-Teller effects [43] and they are properly included in our calculations.

By looking at the wavefunctions of the different states, we realize that the different multiplets can be correlated to the atomic electron configurations. The ground  $^1A_{1g}$  multiplet is the only one coming from the  $6s^2$  electron configuration and the first excited multiplet, 1  $^3T_{1u}$ , correlates with the  $6s6p\text{-}^3P$  atomic term. The second excited multiplet, 1  $^1T_{1u}$ , has a large  $6s6p$  configurational character as well, and the rest of the multiplets belong to the  $5d^96s^26p$  electron configuration. However, there is some  $5d^96s^26p$  configurational character in the 1  $^1T_{1u}$  multiplet, around 11%, and the upper lying 3  $^1T_{1u}$  multiplet can also be described as a mixture of  $5d^96s^26p$  (88%) and  $6s6p$  (12%) configurations. This result shows that, even at the spin-orbit free level of calculation, there is a sizable mixing between electronic states related to different electron configurations.

At the ground state there is an enlargement of the Au-Rb distance in the defective crystal with respect to the Cl-Rb distance in the perfect  $\text{RbCl}$  host (3.420 Å vs. 3.295 Å, a 0.125 Å difference). This fact reflects the larger size of the  $\text{Au}^-$  anion as compared to  $\text{Cl}^-$ . With the  $6s \rightarrow 6p$  electron excitation, we find a further increase of the equilibrium distance. Furthermore, a  $5d \rightarrow 6p$  excitation (implicit in the states of the  $5d^96s^26p$  configuration) brings an extra enlargement of the distance, in line with the larger spatial extension of the  $6p$  orbital.

It should be noticed that the active space used in our calculations ( $\text{Au } 5d6s6p6d7s$ ) does not include states belonging to the  $6s7p$  electron configuration. The features related to these states cannot be calculated using it. Transitions to these states have been suggested to be a potential

origin for the D bands in the absorption spectrum of  $\text{RbCl}:\text{Au}^-$  [6–8]. Inclusion of the main  $7p$  MO in the active space is too demanding for these calculations. However, we performed alternative preliminary calculations with a simpler model (a  $(\text{AuRb}_6)^{5+}$  cluster with a  $\text{Au } 6s6p6d7s7p$  active space) and found there that, at the equivalent MS-CASPT2 level of theory, the states related to the  $6s7p$  electron configuration lie very high in energy, more than 12 eV above the ground state. Then, our calculations do not support the hypothesis of  $6s \rightarrow 7p$  excitations as responsible for the D bands.

Using the MS-CASPT2 wavefunctions and energies of the different states, we have done calculations including the spin-orbit coupling effects between all the states coming from the  $6s^2$ ,  $6s6p$  and  $5d^96s^26p$  electron configurations. The calculated spectroscopic constants of the different electronic levels are collected in Table 2. Together with equilibrium geometries, totally symmetric vibrational frequencies and minimum-to-minimum transition energies, we present vertical transition energies at the geometry of the ground 1  $A_{1g}$  level, absorption oscillator strengths of the allowed transitions and composition of the spin-orbit levels in terms of the spin-orbit free multiplets (the latter two calculated at  $R(\text{Au-Rb}) = 3.413$  Å). The energy curves relative to the  $a_{1g}$  vibrational mode are depicted in Fig. 1. In the Table, we include all the levels up to an energy of around 5.5 eV and, above this energy, only the levels that belong to the  $T_{1u}$  irrep of the  $O_h^*$  double point group (we will use Mulliken's notation for the many-electron states of the cluster throughout this paper). By symmetry arguments, only  $A_{1g} \rightarrow T_{1u}$  transitions are electric dipole allowed in this material. In Fig. 1, which depicts all calculated levels,  $T_{1u}$  levels are highlighted using thick red curves. A larger Table, which recollects data for all the calculated levels, can be found in the supplementary material accompanying this paper [44].

The ground level, 1  $A_{1g}$ , is well separated from the excited levels. At some 4.0–4.5 eV, we find a first manifold of excited levels (1  $A_{1u}$ –1  $E_u$ ). It consists of four levels and all of them have a large contribution from the 1  $^3T_{1u}$ - $6s6p$  multiplet, related to the  $^3P$  atomic term. They can be related to the  $^3P_0$  (1  $A_{1u}$ ),  $^3P_1$  (1  $T_{1u}$ ), and  $^3P_2$  (1  $T_{2u}$ , 1  $E_u$ ) atomic multiplets of  $\text{Au}^-$ . However, we can see from the Table that the levels present a mixing with some higher lying multiplets, of main  $5d^96s^26p$  character. This mixing, due to the spin-orbit coupling, is not very extensive in these levels. The 1  $T_{1u}$  level has a contribution of the spin-orbit free 1  $^1T_{1u}$ -mainly  $6s6p$  multiplet of around 6%. Apart from this, these levels show very dominant triplet character. Note that the splitting of the  $^3P_2$  multiplet due to the octahedral crystal field is very small, amounting to only 8 meV. A substantially larger splitting of this atomic level has been suggested in the literature to explain some of the experimental features of the  $C'$  emission in the title material [8], and in  $\text{KCl}:\text{Au}^-$  [45,46]. Our calculations do not support this explanation.

Above this first manifold of excited states, our calculations show a second one, located around 5.2–5.4 eV and composed of six different levels (1  $A_{2u}$ –2  $E_u$ ). Two of these levels, 2  $T_{1u}$  and 3  $T_{1u}$  correspond to mixtures of the spin-orbit free 1  $^1T_{1u}$  multiplet (mainly  $6s6p$  character) with several higher lying multiplet, of  $5d^96s^26p$  character. The mixing is very extensive and the levels are clearly multiconfigurational in nature. These two levels, separated by some 0.07 eV, present large absorption oscillator strengths. The spin mixing is also very large in these states and the relatively large oscillator strength should reflect the partially allowed configurational ( $6s \rightarrow 6p$ ) and spin (singlet to singlet) character of these transitions. The rest of the levels in this manifold can be described as extensive mixtures of several  $5d^96s^26p$  multiplets, including a large spin mixing as well. This extensive mixing of a number of spin free multiplets, either singlet or triplet, precludes a direct assignment of the levels to atomic terms.

The rest of the calculated levels span a large energy window (5.8–7.8 eV). In general, these levels can be characterized as very large mixings of different  $5d^96s^26p$  multiplets (see Fig. 1 and supplementary information). In Table 2 we collect the information pertaining to the levels of  $T_{1u}$  symmetry. Some of these levels present large oscillator

**Table 2**

Calculated spectroscopic constants of some selected SO levels of the  $\text{Au}^-$  center in  $\text{RbCl}$ . Spin-orbit RASSI-SO calculations. Au-Rb equilibrium distances,  $R_e$ , in Å; totally symmetric vibrational frequencies,  $\nu_{a1g}$ , in  $\text{cm}^{-1}$ ; minimum-to-minimum transition energies,  $T_e$ , in eV; vertical transition energies at the ground state equilibrium distance, in eV; absorption oscillator strengths  $f_{abs}$ ; analysis of the wavefunctions in terms of spin-orbit free multiplets (only contributions larger than 5% are shown).

Level	$R_e$	$\nu_{a1g}$	$T_e$	Absorption <sup>a</sup>	$f_{abs}$ <sup>b</sup>	Percentage contributions of spin-orbit free multiplets <sup>b</sup>
1 $A_{1g}$	3.420	81	0	0		100.00 1 $A_{1g}$
1 $A_{1u}$	3.472	78	3.983	4.000		97.74 1 $^3T_{1u}$
1 $T_{1u}$	3.473	78	4.111	4.128	0.095	92.51 1 $^3T_{1u}$ 6.05 1 $^1T_{1u}$
1 $T_{2u}$	3.499	79	4.420	4.458		88.36 1 $^3T_{1u}$ 8.11 2 $^3T_{1u}$
1 $E_u$	3.500	79	4.426	4.466		89.24 1 $^3T_{1u}$ 7.09 2 $^3T_{1u}$
1 $A_{2u}$	3.522	81	5.182	5.253		42.67 1 $^3T_{2u}$ 38.63 1 $^1A_{2u}$ 18.71 2 $^3T_{2u}$
2 $T_{1u}$	3.512	78	5.223	5.273	0.39	37.00 1 $^1T_{1u}$ 21.16 1 $^3T_{2u}$ 19.76 2 $^1T_{1u}$ 9.33 3 $^3T_{1u}$
						6.67 1 $^3E_u$
2 $T_{2u}$	3.516	81	5.214	5.278		26.42 3 $^3T_{1u}$ 22.90 1 $^1T_{2u}$ 18.95 1 $^3A_{2u}$ 9.52 2 $^1T_{2u}$
						7.66 1 $^3E_u$ 6.77 2 $^3T_{1u}$ 6.53 2 $^3T_{2u}$
3 $T_{1u}$	3.489	81	5.309	5.340	0.68	53.82 1 $^1T_{1u}$ 15.54 1 $^3T_{2u}$ 11.96 2 $^1T_{1u}$ 8.33 3 $^3T_{1u}$
3 $T_{2u}$	3.521	80	5.361	5.425		51.25 2 $^3T_{1u}$ 11.89 1 $^3E_u$ 10.64 2 $^3T_{2u}$ 10.41 1 $^3T_{1u}$
						5.55 1 $^1T_{2u}$
2 $E_u$	3.520	79	5.377	5.440		51.95 2 $^3T_{1u}$ 18.78 2 $^3T_{2u}$ 10.42 1 $^3T_{1u}$ 8.52 1 $^1E_u$
						5.88 3 $^3T_{1u}$
4 $T_{1u}$	3.523	81	5.868	5.940	0.0017	61.22 3 $^3T_{1u}$ 35.71 1 $^3T_{2u}$
5 $T_{1u}$	3.537	80	6.227	6.314	0.17	33.97 2 $^3T_{2u}$ 28.02 2 $^1T_{1u}$ 26.33 1 $^3E_u$ 7.72 2 $^3T_{1u}$
6 $T_{1u}$	3.534	80	6.310	6.396	0.39	48.97 2 $^3T_{1u}$ 27.01 1 $^3E_u$ 16.74 3 $^1T_{1u}$
7 $T_{1u}$	3.516	80	7.073	7.132	0.94	61.97 3 $^1T_{1u}$ 21.07 2 $^3T_{2u}$ 6.30 2 $^1T_{1u}$ 6.15 2 $^3T_{1u}$
8 $T_{1u}$	3.534	81	7.496	7.582	0.0016	27.58 2 $^1T_{1u}$ 24.79 1 $^3E_u$ 23.13 1 $^3T_{2u}$ 13.06 2 $^3T_{1u}$
						8.70 3 $^3T_{1u}$
9 $T_{1u}$	3.541	80	7.653	7.750	0.14	41.69 2 $^3T_{2u}$ 17.49 2 $^3T_{1u}$ 15.55 3 $^1T_{1u}$ 8.22 1 $^3E_u$
						7.62 3 $^3T_{1u}$ 5.36 2 $^1T_{1u}$

<sup>a</sup> Calculated at  $R(\text{Au-Rb}) = 3.420$  Å.

<sup>b</sup> Calculated at  $R(\text{Au-Rb}) = 3.413$  Å.

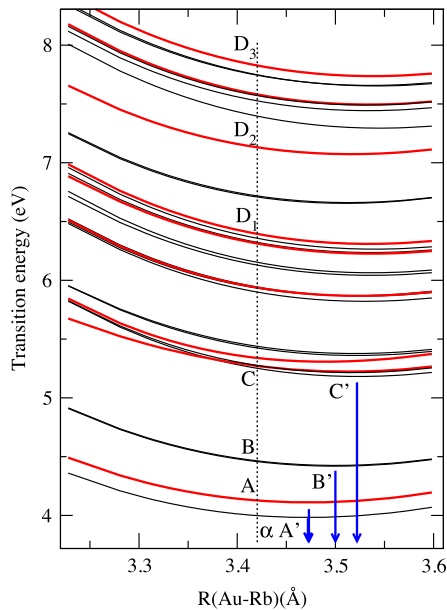


**Fig. 1.** Configuration coordinate energy diagram showing the excited levels of the  $\text{Au}^-$  center in  $\text{RbCl}$ . RASSI-SO spin-orbit results. At this scale, the curve of the ground  $^1A_{1g}$  level is not plotted. Thick red lines represent levels belonging to the  $T_{1u}$  irrep. The dotted line is just a vertical at the ground  $A_{1g}$  level equilibrium distance  $R(\text{Au-Rb}) = 3.420$  Å. Blue arrows represent the different emission bands.

strengths, but we do not find a clear correlation with the singlet character of the level.

To our knowledge, there are not measurements of the equilibrium Au-Rb distance or the breathing vibrational mode frequency for any of the states of this  $\text{Au}^-$  center in  $\text{RbCl}$ . Our calculations predict a loose correlation of the equilibrium distances with the configurational character and a very similar value of the vibrational  $a_{1g}$  frequency for all the levels, which may be a reflection of the weak electron-phonon interac-

tion present in the material. From an analysis of the vibronic structures of the  $A'$  emission, a value of 11 meV ( $89 \text{ cm}^{-1}$ ) [7] is reported for the vibronic maxima in the ground state of  $\text{RbCl}:\text{Au}^-$ . This results is in qualitative agreement with our calculated value for the  $a_{1g}$  frequency,  $81 \text{ cm}^{-1}$ .

### 3.1. Comparison with experiments

Next we present a comparison of our calculated *ab initio* results with the available experimental results and discuss on the assignments of some of the experimental bands. The data necessary for this comparison are presented in Tables 2 and 3, and in Figs. 1 and 2.

Experiments on absorption and emission spectra of  $\text{RbCl}:\text{Au}^-$  were conducted on Ref. [7] and more recently on Ref. [8]. Both of them described a series of bands in the spectra that we are discussing now, focusing on the absorption spectrum first and then on the emission.

The calculated profile of the absorption spectrum is shown in Fig. 2. It has been calculated using a common totally symmetric vibrational frequency of  $80 \text{ cm}^{-1}$  for all the states and a broadening factor of  $15 \text{ cm}^{-1}$ , in the theoretical framework of Refs. [47,48]. The different bands in the spectrum have been labeled according to the experiment [8]. For comparison, we have also plotted the experimental 8 K absorption spectrum, directly taken from Fig. 1(a) of Ref. [8]. The calculated profile has been shifted in energy and scaled so that maximum of the C absorption band coincides in both plots. The agreement of the calculated and the experimental absorption spectrum is very satisfactory.

In the experiments, the first band found in the spectrum (band A) is assigned to the transition from the ground state to the  $^3P_1$  multiplet [7,8]. From our calculation, we assign it to the transition to the spin-orbit  $1 T_{1u}$  level, a level that is mainly related to the  $1 ^3T_{1u}(^3P_1)$  spin free multiplet. Our calculations support the previous assignment. The calculated value of the transition energy shows an overestimation of 0.15 eV, around 4% of the transition, in line with the results of similar calculations on different systems [26,12,11].

Next in increasing energy, a very weak absorption band named B has been found [7], but it is not reported in absorption experiments in Ref. [8]. However, in the excitation spectrum of the  $B'$  emission, a



**Table 3**

Vertical absorption and emission transition energies between some selected electronic levels of the Au<sup>-</sup> center in RbCl. Spin-orbit RASSI-SO calculations. Comparison with available experiments. All energies are in eV. Absorption oscillator strengths,  $f_{abs}$  and radiative lifetimes of the levels<sup>d</sup>,  $\tau$ , in ns.

Level	Absorption				Emission			$\tau$	
	Band	Theory	Exp. <sup>a</sup>	$f_{abs}$ <sup>b</sup>	Band	Theory	Exp. <sup>a</sup>	Theory	Exp. <sup>a</sup>
1 A <sub>1g</sub>		4.00			$\alpha$	3.97	3.81, 3.75 <sup>c</sup>		
1 T <sub>1u</sub>	A	4.13	3.98	0.095	A'	4.09	3.91	15	94
1 T <sub>2u</sub>	B	4.46	4.25		B'	4.38	4.12		11000
1 E <sub>u</sub>		4.47							
1 A <sub>2u</sub>		5.25			C'	5.12	5.00		458
2 T <sub>1u</sub>	C, (d)	5.27		0.39				6.8	
3 T <sub>1u</sub>	C	5.34	5.27	0.68				0.94	
4 T <sub>1u</sub>		5.94		0.0017					
5 T <sub>1u</sub>	D <sub>1</sub>	6.31	5.98	0.17					
6 T <sub>1u</sub>		6.40		0.39					
7 T <sub>1u</sub>	D <sub>2</sub>	7.13	6.90	0.94					
8 T <sub>1u</sub>		7.58		0.0016					
9 T <sub>1u</sub>	D <sub>3</sub>	7.75	7.20	0.14					

<sup>a</sup> Ref. [8].

<sup>b</sup> Calculated at  $R(\text{Au-Rb}) = 3.413 \text{ \AA}$ .

<sup>c</sup> Ref. [7].

<sup>d</sup> Corrected for local field effects [41,42].

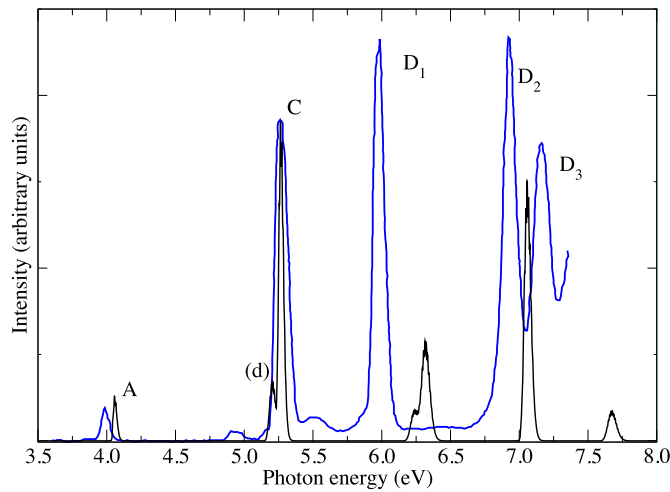


**Fig. 2.** Absorption spectrum profile of the Au<sup>-</sup>-center in RbCl. Black line: present calculation (shifted in energy). Blue line: experimental 8 K absorption spectrum taken from Fig. 1(a) of Ref. [8].

band in this energy range is found and assign to this B band. It is assigned to the transition to the  $^3P_2$  atomic multiplet. In our calculations, two electronic levels,  $1 T_{2u}$  and  $1 E_u$ , are found at 4.46 eV from the ground state, the  $1 T_{2u}$  level lying lowest by only 8 meV. The transitions  $1 A_{1g} \rightarrow 1 T_{2u}$ ,  $1 E_u$  are electric dipole forbidden on symmetry grounds and should be very weak then. We assign the B band to these transitions, supporting the experimental assignment. As described earlier, these levels have a significant contribution from  $5d^9 6s^2 6p$  electron configuration. The position of this band is again overestimated in our calculations by around 0.20 eV.

Another band, called C, is reported in the experimental absorption spectrum at 5.27 eV above the ground state [7,8]. It is a very intense band and its halfwidth is twice that of the A band. Both in the absorption and excitation of the C' emission [8], this band present a shoulder on its low energy side. In the absorption spectrum of KCl: Au<sup>-</sup>, a weak band, called the d band, is reported on this low energy side of the C band [45,9], shifted around 0.2 eV to the red. Several electronic levels are located at this energy (see Table 2) and, with this information in mind, we assign the C absorption band to transitions between the ground level and the  $2 T_{1u}$  and  $3 T_{1u}$  levels. These two levels lie quite close in energy, separated by around only 0.07 eV. Both transitions have

a large oscillator strength so the combined band should be very intense. From Table 2, we see that the difference in the equilibrium geometry of the cluster in these states and in the ground state is relatively large (around 0.70-0.90 Å), a fact that can explain the width of the band. The ordering of the levels in KCl: Au<sup>-</sup> can be expected to be similar to that of RbCl: Au<sup>-</sup> and, based on this, we tentatively assign the d band in the absorption spectrum of KCl: Au<sup>-</sup> to the  $1 A_{1g} \rightarrow 2 T_{1u}$  transition and the C band to the  $1 A_{1g} \rightarrow 3 T_{1u}$  transition.

As discussed above, both  $2 T_{1u}$  and  $3 T_{1u}$  levels can be characterized as multiconfigurational states, having a similar contribution of  $6s 6p$  and  $5d^9 6s^2 6p$  electron configurations, together with a large mixing of singlet and triplet multiplets. In the literature, the C band is assigned to a transition to the atomic  $^1P_1$  multiplet, but our calculations show that this interpretation can be too simplistic. The difference between the experimental and calculated transition energies is smaller than for A and B bands, around 0.07 eV.

At higher energies, three more intense bands are found in the absorption spectrum at low temperature (8 K) [8], labeled D<sub>1</sub>, D<sub>2</sub>, and D<sub>3</sub> in order of increasing energy. The origin of these transitions was not firmly established from the experiments, and  $5d^{10} 6s^2 \rightarrow 5d^9 6s^2 6p$  or  $6s^2 \rightarrow 6s 7p$  transitions [6–8] have been suggested as hypothetical explanations. From our calculations, we assign these bands to transitions from the  $1 A_{1g}$  ground level to the  $5 T_{1u}$ ,  $6 T_{1u}$ ,  $7 T_{1u}$ , and  $9 T_{1u}$  levels, respectively. All these electronic levels mainly belong to the  $5d^9 6s^2 6p$  electronic configuration (see Tables 1 and 2), so that our calculations strongly support the assignment of these D bands to  $5d \rightarrow 6p$  electron transitions.

Both in the absorption (8 K) and the excitation of the C' emission, band D<sub>1</sub> seems to be a complex band, with a shoulder in its low energy side. Its intensity is comparable to that of the C band. All these features nicely agree with our assignment of the band to transitions to the  $5 T_{1u}$ ,  $6 T_{1u}$  electronic levels, separated by some 0.09 eV in our calculations. It should be noted that an analogous band is reported in the spectra of KCl: Au<sup>-</sup>, and it presents a small band in the low-energy tail [45]. On the other hand, we assign band D<sub>2</sub> to the  $1 A_{1g} \rightarrow 7 T_{1u}$  transition. This transition presents the largest value of the absorption strength. Finally, band D<sub>3</sub>, visible in the 8 K absorption spectrum and the excitation spectrum of the B' emission, is assigned to the  $1 A_{1g} \rightarrow 9 T_{1u}$  transition. Its oscillator strength is around 6.5 times smaller than the  $1 A_{1g} \rightarrow 7 T_{1u}$  transition (origin of the D<sub>2</sub> band), in qualitative agreement with the intensities in the excitation spectra of the title material [8]. As in the other transitions, our calculations overestimate the transition energies for the D bands. In this case, the overestimation is larger than for the rest of the bands, ranging from 0.23 eV (D<sub>2</sub> band) to 0.55 eV (D<sub>3</sub> band).

Two more electric dipole allowed transitions are predicted from our calculations, to the  $5d^96s^26p$ -related  $4\ T_{1u}$  and  $8\ T_{1u}$  levels. However, the oscillator strengths of these transitions are 2 orders of magnitude smaller than for the above commented bands. This justifies that no further bands appear in the absorption spectrum. To our knowledge, oscillator strengths have not been reported for the transitions in  $\text{RbCl:Au}^-$ . However, they have been estimated for  $\text{KCl:Au}^-$  [45]. Our calculated values are (except for the d band) of the same order of magnitude.

We will discuss now on the emission spectrum of  $\text{RbCl:Au}^-$ . This emission spectrum has been reported recently [8] and the results agree with the data reported previously [7]. The experiment shows a relatively complex emission for the material, in which the number of bands strongly depends on the excitation energy and the temperature. This is due to the interplay of radiative and radiationless processes that occur after excitation. Our calculations give information about the radiative processes only, and we will focus on them. In Table 3, we present the vertical transition energies from the equilibrium geometry of the cluster in the different excited states involved in the emission together with the experimental values of the maxima of the emission bands. We present as well the calculated radiative lifetimes of the electronic states.

The emission spectrum of the  $\text{Au}^-$  center in  $\text{RbCl}$ , after excitation at 6.89 eV (i.e. into the  $D_2$  band) at 8 K shows four bands [8]. In increasing energy, the first one is a weak band referred to as  $\alpha$ . This band is assigned to the  $^3P_0 \rightarrow ^1S_0$  transition. Our calculations suggest the assignment of this band to the  $1\ A_{1u} \rightarrow 1\ A_{1g}$  transition, in agreement with the experiment. This transition is electric dipole forbidden and, hence very weak. The discrepancy between the calculated and experimentally measured transition energies is around 0.15 eV, in line with the discrepancies found in absorption and the rest of the emission lines. Next in energy lie two bands named  $A'$  and  $B'$ . According to our calculations, these are the inversions of A and B absorptions, respectively. This assignment supports the experimental assignments of these bands. The difference between the maxima of the A absorption and the  $A'$  emission is small, around 0.04 eV, also smaller than the experimental value (0.09 eV). The transition that gives origin to the  $A'$  band ( $1\ T_{1u} \rightarrow 1\ A_{1g}$ ) is electric dipole allowed and the calculated radiative lifetime of the  $1\ T_{1u}$  level is of 15 ns. This value is similar to the experimental value of 94 ns [8]. A zero phonon line is reported for the  $A'$  band in Ref. [7] at 3.948 eV. From Table 2, the minimum-to-minimum transition energy is 4.111 eV, in good agreement with the experiment.

The situation is somewhat more complicated with respect to the  $C'$  luminescence. Experimentally, it is found that the state responsible for the  $C'$  emission is not the same as the one responsible for the C absorption. The decay time of the level is very large for a dipole allowed transition [8]. The main explanation assumes the presence an electronic level just below the C absorbing state (a “trapped” level) [8]. The same situation is reported for the  $C'$  luminescence of  $\text{KCl:Au}^-$  [7,45,9]. Several origins have been suggested in the literature for this level. In Refs. [8,45,46], this level is supposed to be the  $1\ T_{2u}$  level coming from the octahedral splitting of the  $^3P_2$  atomic multiplet. According to Ref. [7] the level belongs to the  $6s7p$  electron configuration. As we discussed above, our calculations do not support these explanations.

In fact, our calculations show that the origin of the so-called  $C'$  emission is the  $5d^96s^26p\ 1\ A_{2u}$  level. This level is the lowest lying in a manifold of levels that includes the  $2\ T_{1u}$  and  $3\ T_{1u}$ , that we proposed as final states of the d and C absorptions. The  $1\ A_{2u}$  level lies only 20 meV below the  $2\ T_{1u}$  level. After the  $D_2$  excitation, the system can undergo radiationless transitions to this metastable state that emit afterwards. The transition energy from this level is about 5.12 eV, in good agreement with the experiment. On the other hand, the  $1\ A_{2u} \rightarrow 1\ A_{1g}$  is electric dipole forbidden and this can explain the relative large decay time of the luminescence. The small energy difference with the  $2\ T_{1u}$  (the d state) suggests that, with increasing temperature, the upper level can increase its population and, as the emission from it is allowed, shorten the decay time of the band found experimentally. Then, the  $1\ A_{2u}$  level may be regarded as a “trapped” level, as suggested by

the experimental explanations. Note that the calculated radiative lifetimes of the  $2\ T_{1u}$  and  $3\ T_{1u}$  levels are short, in the range expected for electric dipole allowed transitions and thus, their values disagree with the measured decay time.

#### 4. Conclusions

We have performed *ab initio* wavefunction based theoretical calculations on a  $(\text{AuRb}_6\text{Cl}_{12})^{7-}$  cluster embedded in a AIMP model potential in order to study the electronic structure and optical spectra of the  $\text{Au}^-$  center in  $\text{RbCl}$  crystals. The calculated energies and oscillator strengths of the different electronic transitions provide a detailed description of the absorption and emission spectra of the material, in very good agreement with experimentally determined quantities.

The different features of the absorption spectrum have been accurately reproduced by the calculations. A new assignment is given for band C in the absorption spectrum, assigned in the literature to a transition to the  $^1P_1$  atomic multiplet. We find that two electronic levels,  $2\ T_{1u}$  and  $3\ T_{1u}$ , which are multiconfigurational in nature (extensive mixings of  $6s6p$  and  $5d^96s^26p$  configurations) and present large mixings of singlet and triplet multiplets, are the final states of the transitions. According to the calculations, the transition to the  $2\ T_{1u}$  level may be responsible for the d band found for  $\text{Au}^-$  centers in  $\text{KCl}$  crystals. The three D bands present in the low temperature absorption spectrum of the material are assigned to allowed transitions to different  $5d^96s^26p$  levels belonging to the  $T_{1u}$  irrep. The explanation of these bands as  $6s \rightarrow 7p$  transitions is not supported by our calculations.

With respect to the emission spectrum, our calculation agrees with the origin and properties of the  $\alpha$ ,  $A'$ , and  $B'$  bands given in the experiment, the agreement being very satisfactory. We propose a new assignment for the  $C'$  band. The initial state is the  $1\ A_{2u}$  level that is found just below the  $2\ T_{1u}$  and  $3\ T_{1u}$  levels responsible for the C absorption (some 0.020 eV below). This level may act as the “trapped” level invoked in the experiments in order to explain the characteristics of this emission. With this origin, our calculations do not give support to the alternative suggestions found in the literature, as the  $1\ A_{2u}$  level can be described as a  $5d^96s^26p$  configurational level.

In summary, our calculations provide solid information that can help solving some of the uncertainties that still exist in the interpretation of the optical spectrum of  $\text{Au}^-$  centers in alkali halides.

#### Declaration of competing interest

The authors declare that they have no known competing financial interests or personal relationships that could have appeared to influence the work reported in this paper.

#### Data availability

Data will be made available on request.

#### Acknowledgements

The author gratefully acknowledges Zoila Barandiarán and Luis Seijo for continuous support for many years. This work was partly supported by a grant from Ministerio de Economía y Competitividad, Spain (Dirección General de Investigación y Gestión del Plan Nacional de I+D+i, MAT2017-83553-P).

#### Appendix A. Supplementary material

Supplementary material related to this article can be found online at <https://doi.org/10.1016/j.jlumin.2023.120207>.

## References

- [1] R. Hilsch, Die Absorptionsspektren einiger Alkali-Halogenid-Phosphore mit Tl- und Pb-Zusatz, *Z. Phys.* 44 (11–12) (1927) 860–870, <https://doi.org/10.1007/BF01390859>.
- [2] F. Seitz, Interpretation of the properties of alkali halide-thallium phosphors, *J. Chem. Phys.* 6 (3) (1938) 150–162, <https://doi.org/10.1063/1.1750216>.
- [3] A. Fukuda, Alkali halide phosphors containing impurity ions with (s)2 configurations, *Sci. Light* 13 (1964) 64–114.
- [4] A. Ranfagni, D. Mugnai, M. Bacci, G. Viliani, M.P. Fontana, The optical properties of thallium-like impurities in alkali-halide crystals, *Adv. Phys.* 32 (6) (1983) 823–905, <https://doi.org/10.1080/00018738300101621>.
- [5] P.W.M. Jacobs, Alkali halide crystals containing impurity ions with the ns2 ground-state electronic configuration, *J. Phys. Chem. Solids* 52 (1) (1991) 35–67, [https://doi.org/10.1016/0022-3697\(91\)90059-9](https://doi.org/10.1016/0022-3697(91)90059-9).
- [6] T. Mabuchi, A. Yoshikawa, R. Onaka, Absorption spectra of Au<sup>+</sup> ions in Alkali Halides, *J. Phys. Soc. Jpn.* 28 (1970) 805.
- [7] M. Krause, F. Fischer, Au, Luminescence in Alkali Halides, *J. Lumin.* 4 (1971) 335–344.
- [8] S. Yamasu, T. Kawai, Electronic states and relaxation dynamics of Au<sup>+</sup> centers in RbCl crystals, *J. Lumin.* 236 (March 2021) 118094, <https://doi.org/10.1016/j.jlumin.2021.118094>.
- [9] K. Shigematsu, R. Onaka, Luminescence properties of Au<sup>+</sup> center in KCl, *Sci. Light* 23 (2) (1974) 27–42.
- [10] G. Blasse, Classical phosphors: a Pandora's box, *J. Lumin.* 72–74 (1997) 129–134, [https://doi.org/10.1016/S0022-2313\(96\)00166-4](https://doi.org/10.1016/S0022-2313(96)00166-4).
- [11] Z. Barandiarán, J. Joos, L. Seijo, Luminescent Materials, Springer Series in Materials Science, vol. 322, Springer, 2022.
- [12] J.L. Pascual, Ab initio calculations of the electronic structure of red-emitting Mn<sup>4+</sup>-doped fluorides, *J. Phys. Chem. C* 123 (2019) 27150–27164, <https://doi.org/10.1021/acs.jpcc.9b08245>.
- [13] M.D. Jong, A. Meijerink, R.A. Gordon, Z. Barandiarán, L. Seijo, Is Bi<sup>2+</sup> responsible for the red-orange emission of bismuth-doped SrB<sub>4</sub>O<sub>7</sub>, *J. Phys. Chem. C* 118 (2014) 9696–9705, <http://pubs.acs.org/doi/abs/10.1021/jp502996t>.
- [14] B.O. Roos, P.R. Taylor, P.E.M. Siegbahn, A complete active space SCF (CASSCF) method using a density matrix formulated super-CI approach, *Chem. Phys.* 48 (1980) 157–173.
- [15] P.E.M. Siegbahn, A. Heiberg, B.O. Roos, B. Levy, A comparison of the super-CI and the Newton-Raphson scheme in the complete active space SCF method, *Phys. Scr.* 21 (1980) 323–327.
- [16] P.E.M. Siegbahn, J. Almlof, A. Heiberg, B.O. Roos, The complete active space SCF (CASSCF) method in a Newton-Raphson formulation with application to the HNO molecule, *J. Chem. Phys.* 74 (4) (1981) 2384, <https://doi.org/10.1063/1.441359>, <http://link.aip.org/link/?JCP/74/2384/1&Agg=doi>.
- [17] K. Andersson, P.-Å. Malmqvist, B.O. Roos, A.J. Sadlej, K. Wolinski, Second-order perturbation theory with a CASSCF reference function, *J. Phys. Chem.* 94 (14) (1990) 5483–5488, <https://doi.org/10.1021/j100377a012>.
- [18] K. Andersson, P.-Å. Malmqvist, B.O. Roos, Second-order perturbation theory with a complete active space self-consistent field reference function, *J. Chem. Phys.* 96 (2) (1992) 1218–1226, <https://doi.org/10.1063/1.462209>.
- [19] A. Zaitsevskii, J.P. Malrieu, Multi-partitioning quasidgenerate perturbation theory. A new approach to multireference Møller-Plesset perturbation theory, *Chem. Phys. Lett.* 233 (5–6) (1995) 597–604, [https://doi.org/10.1016/0009-2614\(94\)01503-N](https://doi.org/10.1016/0009-2614(94)01503-N).
- [20] J. Finley, P.-Å. Malmqvist, B.O. Roos, L. Serrano-Andrés, The multi-state CASPT2 method, *Chem. Phys. Lett.* 288 (2–4) (1998) 299–306, [https://doi.org/10.1016/S0009-2614\(98\)00252-8](https://doi.org/10.1016/S0009-2614(98)00252-8).
- [21] M. Douglas, N.M. Kroll, Quantum electrodynamical corrections to the fine structure of Helium, *Ann. Phys.* 155 (1974) 89–155.
- [22] B. Hess, Relativistic electronic-structure calculations employing a two-component no-pair formalism with external field projection operators, *Phys. Rev. A* 33 (6) (1986) 3742–3748.
- [23] B. Hess, C. Marian, U. Wahlgren, O. Gropen, A mean-field spin-orbit method applicable to correlated wavefunctions, *Chem. Phys. Lett.* 251 (5–6) (1996) 365–371, [https://doi.org/10.1016/0009-2614\(96\)00119-4](https://doi.org/10.1016/0009-2614(96)00119-4), <http://linkinghub.elsevier.com/retrieve/pii/S0009261496001194>.
- [24] P.-Å. Malmqvist, B.O. Roos, B. Schimmelpfennig, The restricted active space (RAS) state interaction approach with spin-orbit coupling, *Chem. Phys. Lett.* 357 (3–4) (2002) 230–240, [https://doi.org/10.1016/S0009-2614\(02\)00498-0](https://doi.org/10.1016/S0009-2614(02)00498-0), <http://linkinghub.elsevier.com/retrieve/pii/S0009261402004980>.
- [25] Z. Barandiarán, L. Seijo, The ab initio model potential representation of the crystalline environment. Theoretical study of the local distortion on NaCl:Cu<sup>+</sup>, *J. Chem. Phys.* 89 (9) (1988) 5739–5746, <https://doi.org/10.1063/1.455549>.
- [26] L. Seijo, Z. Barandiarán, The ab initio model potential method: a common strategy for effective core potential and embedded cluster calculations, in: J. Leszczynski (Ed.), *Computational Chemistry: Reviews of Modern Trends*, vol. 4, World Scientific, Singapore, 1999, pp. 55–152.
- [27] F. Aquilante, J. Autschbach, R.K. Carlson, L.F. Chibotaru, M.G. Delcey, L. De Vico, I. Fdez Galván, N. Ferré, L.M. Frutos, L. Gagliardi, M. Garavelli, A. Giusani, C.E. Hoyer, G. Li Manni, H. Lischka, D. Ma, P.-Å. Malmqvist, T. Müller, A. Nenov, M. Olivucci, T.B. Pedersen, D. Peng, F. Plasser, B. Pritchard, M. Reiher, I. Rivalta, I. Schapiro, J. Segarra-Martí, M. Stenrup, D.G. Truhlar, L. Ungur, A. Valentini, S. Vancoillie, V. Veryazov, V.P. Vysotskiy, O. Weingart, F. Zapata, R. Lindh, Molcas 8: new capabilities for multiconfigurational quantum chemical calculations across the periodic table, *J. Comput. Chem.* 37 (5) (2016) 506–541, <https://doi.org/10.1002/jcc.24221>.
- [28] K.-H. Hellwege, A.M. Hellwege (Eds.), *Key Elements: F, Cl, Br, I, Landolt-Börnstein - Group III Condensed Matter 7a*, 1st edition, Springer-Verlag, Berlin Heidelberg, 1973.
- [29] D.B. Sirdeshmukh, L. Sirdeshmukh, K.G. Subhadra, Alkali Halides, Springer Series in Materials Science, vol. 49, Springer, 2001.
- [30] B.O. Roos, R. Lindh, P.-Å. Malmqvist, V. Veryazov, P.O. Widmark, New relativistic ANO basis sets for transition metal atoms, *J. Phys. Chem. A* 109 (29) (2005) 6575–6579, <https://doi.org/10.1021/jp0581126>.
- [31] B.O. Roos, V. Veryazov, P.O. Widmark, Relativistic atomic natural orbital type basis sets for the alkaline and alkaline-Earth atoms applied to the ground-state potentials for the corresponding dimers, *Theor. Chem. Acc.* 111 (2–6) (2004) 345–351, <https://doi.org/10.1007/s00214-003-0537-0>.
- [32] B.O. Roos, R. Lindh, P.-Å. Malmqvist, V. Veryazov, P.O. Widmark, Main group atoms and dimers studied with a new relativistic ANO basis set, *J. Phys. Chem. A* 108 (15) (2004) 2851–2858, <https://doi.org/10.1021/jp031064>.
- [33] J.L. Pascual, L. Seijo, Z. Barandiarán, Ab initio model potential study of environmental effects on the Jahn-Teller parameters of Cu<sup>2+</sup> and Ag<sup>2+</sup> impurities in MgO, CaO, and SrO hosts, *J. Chem. Phys.* 98 (12) (1993) 9715–9725.
- [34] A. Gellé, M.-B. Lepetit, Fast calculation of the electrostatic potential in ionic crystals by direct summation method, *J. Chem. Phys.* 128 (24) (2008) 244716, <https://doi.org/10.1063/1.2931458>, <http://www.ncbi.nlm.nih.gov/pubmed/18601374>.
- [35] P.P. Ewald, Die Berechnung Optischer und Elektrostatischer Gitterpotentiale, *Ann. Phys.* 64 (1921) 253.
- [36] G. Ghigo, B.O. Roos, P.-Å. Malmqvist, A modified definition of the zeroth-order Hamiltonian in multiconfigurational perturbation theory (CASPT2), *Chem. Phys. Lett.* 396 (1–3) (2004) 142–149, <https://doi.org/10.1016/j.cplett.2004.08.032>.
- [37] N. Forsberg, P.-Å. Malmqvist, Multiconfiguration perturbation theory with imaginary level shift, *Chem. Phys. Lett.* 274 (1–3) (1997) 196–204, [https://doi.org/10.1016/S0009-2614\(97\)00669-6](https://doi.org/10.1016/S0009-2614(97)00669-6).
- [38] R. Llusar, M. Casarubios, Z. Barandiarán, L. Seijo, Ab initio model potential calculations on the electronic spectrum of Ni<sup>2+</sup>-doped MgO including correlation, spin-orbit and embedding effects, *J. Chem. Phys.* 105 (13) (1996) 5321–5330, <https://doi.org/10.1063/1.472376>.
- [39] J. Oddershede, Present state of the calculation of radiative lifetimes of molecules, *Phys. Scr.* 20 (5–6) (1979) 587–593, <https://doi.org/10.1088/0031-8949/20/5-6/005>, <http://stacks.iop.org/1402-4896/20/i=5-6/a=005?key=crossref.96201688ae354b324dbfe475b8ad2dcf>.
- [40] R.C. Hilborn, Einstein coefficients, cross sections, f values, dipole moments, and all that, *Am. J. Phys.* 50 (11) (1982) 982–986, <https://doi.org/10.1119/1.12937>, [arXiv:physics/0202029](https://arxiv.org/abs/physics/0202029).
- [41] B. Henderson, G.F. Imbusch, *Optical Spectroscopy of Inorganic Solids*, Clarendon Press, Oxford, U.K., 1989.
- [42] J. García Solé, L.E. Bausá, D. Jaque, An Introduction to the Optical Spectroscopy of Inorganic Solids, John Wiley & Sons, 2005.
- [43] D. Lemoyne, J. Duran, M. Billardon, L.S. Dang, Vibronic model for an ns2 system: KCl:Cu, *Phys. Rev. B* 14 (1976) 747.
- [44] See supplementary information for a Table showing spectroscopic constants of all the calculated spin-orbit levels.
- [45] M. Krause, Electronic states and transition probabilities of the Au<sup>+</sup> center in KCl, *J. Lumin.* 10 (6) (1975) 391–410, [https://doi.org/10.1016/0022-2313\(75\)90004-6](https://doi.org/10.1016/0022-2313(75)90004-6).
- [46] D. Lemoyne, Evidence for crystal-field splitting of the 3P2 state in KCl:Cu, *J. Phys. C, Solid State Phys.* 13 (33) (1980) 6189–6195, <https://doi.org/10.1088/0022-3719/13/33/016>.
- [47] E.J. Heller, Time-dependent approach to semiclassical dynamics, *J. Chem. Phys.* 62 (4) (1975) 1544, <https://doi.org/10.1063/1.430620>, <http://scitation.aip.org/content/aip/journal/jcp/62/4/10.1063/1.430620>.
- [48] L. Tutt, D. Tannor, J. Schindler, E.J. Heller, J.I. Zink, Calculation of the missing mode effect frequencies from Raman intensities, *J. Phys. Chem.* 87 (5) (1983) 3017–3019, <http://pubs.acs.org/doi/abs/10.1021/j100239a010>.